Radiation damage on sub-cellular scales: Beyond DNA

HL Byrne[1], AL McNamara[1], W Domanova[1,2], S Guatelli[3] and Z Kuncic[1]

[1] Institute of Medical Physics, School of Physics, University of Sydney, NSW, 2006, Australia

[2] Department of Physics, Technical University of Munich, Germany

[3] Centre for Medical Radiation Physics, University of Wollongong, NSW, 2522, Australia

E-mail: h.byrne@physics.usyd.edu.au

Abstract.

This study investigates a model cell as a target for low-dose radiation using Monte Carlo simulations. Mono-energetic electrons and photons are used with initial energies between 10 and 50 keV, relevant to out-of-field radiotherapy scenarios where modern treatment modalities expose relatively large amounts of healthy tissue to low-dose radiation, and also to microbeam cell irradiation studies which show the importance of the cytoplasm as a radiation target. The relative proportions of number of ionisations and total energy deposit in the nucleus and cytoplasm are calculated. We show that for a macroscopic dose of no more than 1 Gy only a few hundred ionisations occur in the nucleus volume whereas the number of ionisations in the cytoplasm is over a magnitude larger. We find that the cell geometry can have an appreciable effect on energy deposit in the cell and can cause a non-linear increase in energy deposit with cytoplasm density. We also show that changing the nucleus volume has negligible effect on the total energy deposit but alters the relative proportion deposited in the nucleus and cytoplasm; the nucleus volume must increase to approximately the same volume as the cytoplasm before energy deposit in the nucleus matches that in the cytoplasm. Additionally we find that energy deposited by electrons is generally insensitive to spatial variations in chemical composition, which can be attributed to negligible differences in electron stopping power for cytoplasm and nucleus materials. On the other hand, we find that chemical composition can affect energy deposited by photons due to non-negligible differences in attenuation coefficients. These results are of relevance in considering radiation effects in healthy cells, which tend to have smaller nuclei. Our results further show that the cytoplasm and organelles residing therein can be important targets for low-dose radiation damage in healthy cells and warrant investigation as much as the conventional focus of a high-dose radiation DNA target in tumour cells.

Submitted to: *Phys. Med. Biol.*

1. Introduction

Radiation damage inflicted outside the cell nucleus is poorly understood in comparison to damage that occurs on or near nuclear DNA. Yet, a growing body of evidence has emerged to suggest that nuclear DNA is by no means the exclusive radiation target in a cell. Microbeam cell irradiation experiments, in particular, have revealed compelling evidence for cellular responses triggered as a result of intra- and inter-cellular signalling invoked by extra-nuclear irradiation. These include immediate and delayed effects such as radiation-induced bystander effect, genomic instability, radiation hypersensitivity, transgenerational responses and radioadaptive responses (Prise et al., 2005; Rodemann and Blaese, 2007; Ahmed et al., 2008; Prise and O'Sullivan, 2009; Averbeck, 2010; Wright, 2010). Crucially, these responses are observed when only the cytoplasm is irradiated and are independent of dose level and radiation type (Shao, 2004; Chouin et al., 2009; Hei et al., 2009; Schettino et al., 2010). Reactive oxygen and nitrogen species are implicated in the damage-sensing signalling pathways (Shao, 2004; Hamada et al., 2007). Knowledge of the production amount and sites of these free radicals combined with an understanding of their subsequent diffusion and biochemical reactions will give much needed insight into the cellular response pathways that are triggered by the primary action of radiation (Kuncic et al., 2012).

The results from microbeam cell irradiation experiments have potentially significant implications for non-targeted radiation during medical imaging procedures and radiation treatment of cancer. Modern radiotherapy techniques, in particular, expose large volumes of normal tissue to low dose radiation, but there are conflicting views in the literature as to whether conformal radiation delivery and image guidance lead to an increase in secondary cancers (Hall and Wuu, 2003; Hall, 2006). This exemplifies the need for a better understanding of the physical, chemical and biological mechanisms responsible for radiation-induced damage to healthy cells.

The low-dose radiation bath that out-of-field healthy cells are exposed to in a typical external beam radiotherapy treatment is comprised of low-energy photons and electrons, which enter cells from arbitrary directions and have varying penetration depths. Radiobiological models and Monte Carlo simulations (e.g. Elkind, 1985; Prise et al., 2001; Friedland et al., 2003; Bassing and Alt, 2004; Hsiao and Stewart, 2008; Nikjoo et al., 2008; Garty et al., 2010; Francis et al., 2011b; McNamara et al., 2012), are typically developed around the mechanistic action of radiation damage to nuclear DNA and almost exclusively focus on tumour cell death induced by high-dose radiation. Relatively little attention has been paid to modelling the action of radiation in healthy cells exposed to low-dose radiation. Healthy cells generally have a lower nucleus/cytoplasm volume ratio than many cancerous cells (e.g. Watanabe et al., 1983; Battlehner et al., 1993), which can affect the proportion of ionisations that occur outside the nucleus. The spatial distribution of these ionisations and the mean energy deposited in the cell may also be influenced by micron-scale heterogeneities, e.g. spatial variations in chemical composition and density of different substructures

(nucleus, cytosol, organelles, membranes etc.), and therefore can potentially influence which damage-sensing signalling pathways are triggered.

In this paper, we report on a Monte Carlo study to investigate ionisations and energy deposit in a virtual cell model containing a nucleus and cytoplasm with realistic chemical composition. The cell is immersed in a background of low energy photons and electrons emulating an "out-of-field" radiation bath in a typical external beam radiotherapy treatment (e.g. Syme et al., 2009; Chofor et al., 2010). We investigate the number of ionisations as well as changes in particle tracks and energy deposition in the cytoplasm and nucleus when the cellular density and nucleus size are varied.

2. Method

Simulations were developed using the open source Monte Carlo (MC) software toolkit Geant4, version 4.9.4 p01 (Agostinelli et al., 2003; Allison et al., 2006). This was chosen because of the availability of radiation transport physics models appropriate for the micron-scale of the simulations. The cell model consisted of a sphere of radius 5 μm filled with cytoplasm material containing a central spherical nucleus of radius 2 μm filled with nucleus material. The whole cell was suspended in water.

Realistic chemical compositions were used for the nucleus and cytoplasm regions in the cell. The nucleus material was based on the ICRU Report 44 (International Commission on Radiation Units and Measurements (ICRU), 1989). No published data was found on complete cytoplasmic chemical composition, so mass fractions were determined by subtracting the nucleus material from an average of the male and female group 1 soft tissue definitions given in table 3 of White et al. (1987). Values were rounded to 2 decimal places and the largest contributors (oxygen and carbon) were rounded down to allow the values to sum to 100 %. Table 1 shows the resulting chemical composition of the nucleus and cytoplasm materials defined by mass fraction. The number of ionisations and energy deposit in these materials was compared to that in a cell filled with liquid water.

Mono-energetic photons and electrons were injected into the cell from random locations around the cell surface with randomised directions (see figure 1). Particle energies were specified between 10–50 keV, indicative of out-of-field, low-energy secondary radiation in radiotherapy procedures. All incident and secondary particles produced were tracked until they deposited all their energy or left the simulation volume.

Geant4 Low Energy electromagnetic processes were used (Chauvie et al., 2004), allowing production of secondary particles down to a cut-off set to 250 eV and with a range cut-off set at 10 nm, corresponding approximately to the CSDA range of a 250 eV electron (Francis et al., 2011a). The following physics processes were activated: electron ionisation, bremsstrahlung, multiple scattering, the photo-electric effect, Compton scattering, Rayleigh scattering, Auger electron emission and fluorescence. Each process activated in Geant4 allows the user to choose a model encapsulating the physics to be used. The Penelope physics models (Baró et al., 1995; Salvat et al., 2009) were selected

as appropriate for the low-energy, micron-scale environment being simulated, and for their ability to simulate the physics in various materials.

Table 1. Chemical composition of cellular materials by percentage mass fraction.

Material	H	O	C	N	P	Na	S	Cl	K
Water	11.19	88.81	0	0	0	0	0	0	0
Cytoplasm	10.55	56.30	29.88	2.51	0.04	0.11	0.24	0.16	0.21
Nucleus	10.60	74.20	9.00	3.20	2.60	0	0.40	0	0

The total energy deposited was normalised to 3 MeV in a reference cell with density $1.0\,\mathrm{g\,cm^{-3}}$, corresponding to a macroscopic dose in the cell volume of approximately 1 Gy, representative of low-dose, out-of-field secondary radiation (Syme et al., 2009; Chofor et al., 2010). Dose is a macroscopic average quantity not relevant to the micro scale of this study, so we have taken 3 MeV as a typical value for energy deposit in a typical cell. Keeping the number of injected particles at each initial energy fixed, the number of ionisations and energy deposit within the cytoplasm and nucleus regions and corresponding particle track structures were recorded for the following three cases considered:

Case 1 Varying chemical composition — The composition of the materials used in the simulation was changed from realistic cytoplasm and nucleus materials (heterogeneous cell) to liquid water for both regions (homogeneous cell) to investigate the effect on number of ionisations produced.

Case 2 Varying density — To investigate the effect of changing the density of the materials used in the cell model, the nucleus or cytoplasm density was varied between 0.5 and $2.0\,\mathrm{g\,cm^{-3}}$;

Case 3 Varying nucleus volume — To investigate the effect on relative energy deposit in the nucleus and cytoplasm, the nucleus volume was doubled for each simulation until it represented just over half the total cell volume at 8 times the original volume.

As radiation interactions occur stochastically, each simulation produces a slightly different outcome for a given total deposited energy, so numerical experiments were run 80 times for each set of initial conditions to achieve a Standard Error in the Mean (SEM) of $\lesssim 1\,\%$.

2.1. Normalisation in realistic cell

Figure 2 shows the number of particles needed for each incident energy to normalise the total energy deposit in the cell to 3 MeV for the reference cell with density $1.0\,\mathrm{g\,cm^{-3}}$ and with nucleus volume 6.4% of the total cell volume. Figure 3 shows plots of the Geant4 Penelope models for electron stopping power and photon attenuation in the defined cytoplasm and nucleus materials.

Figure 2(a) shows that in the case of electrons with initial energies between 10–20 keV, corresponding to ranges less than the 10 μm cell diameter (Francis et al., 2011a), relatively low numbers of electrons are needed to achieve normalisation because nearly all incident electrons are stopped and deposit all their energy within the cell. At higher energies, electrons experience a lower stopping power (c.f. figure 3(a)) and more are able to traverse and escape from the cell, so progressively more higher energy electrons are needed to deposit the 3 MeV normalisation energy. This effect is illustrated in the track structure visualisations for 20 keV and 40 keV incident electrons shown in figure 1(a) and (b) respectively.

Figure 2(b) shows that in the case of photons, considerably larger numbers of incident particles are needed to attain the 3 MeV energy deposition normalisation because of the very few interactions compared to electrons with the same incident energy (the mean-free-path of a 10 keV photon in water is $\approx$ 0.2 cm). Photoelectric absorption is the major contributor to the total mass attenuation coefficient (μ_m) at photon energies $\lesssim$ 20 keV, while Compton scattering becomes the dominant interaction process at energies $\gtrsim$ 30 keV.

The number of incident photons needed for normalisation increases up to $\simeq$ 40 keV and decreases beyond that incident energy for two reasons. The total μ_m, and in particular the contribution from photo-absorption, drops sharply over the 10–40 keV energy range (c.f. figure 3(b)). In addition, the photo-electrons produced are more likely to traverse and escape from the cell, particularly at higher photon energies, as they have a maximum energy close to the incident photon energy, while Compton recoil electrons have a much lower average energy ($\simeq$ 4 keV for a 50 keV incident photon). These effects are evident in the corresponding track structures for 20 keV and 40 keV incident photons shown in figure 1(c) and (d). At energies $\simeq$ 40 keV the photo-absorption becomes negligible while the attenuation coefficient for Compton scattering remains relatively constant (c.f. figure 3(b)), so the number of incident photons needed for normalisation drops with the increasing average energy of the Compton recoil electrons.

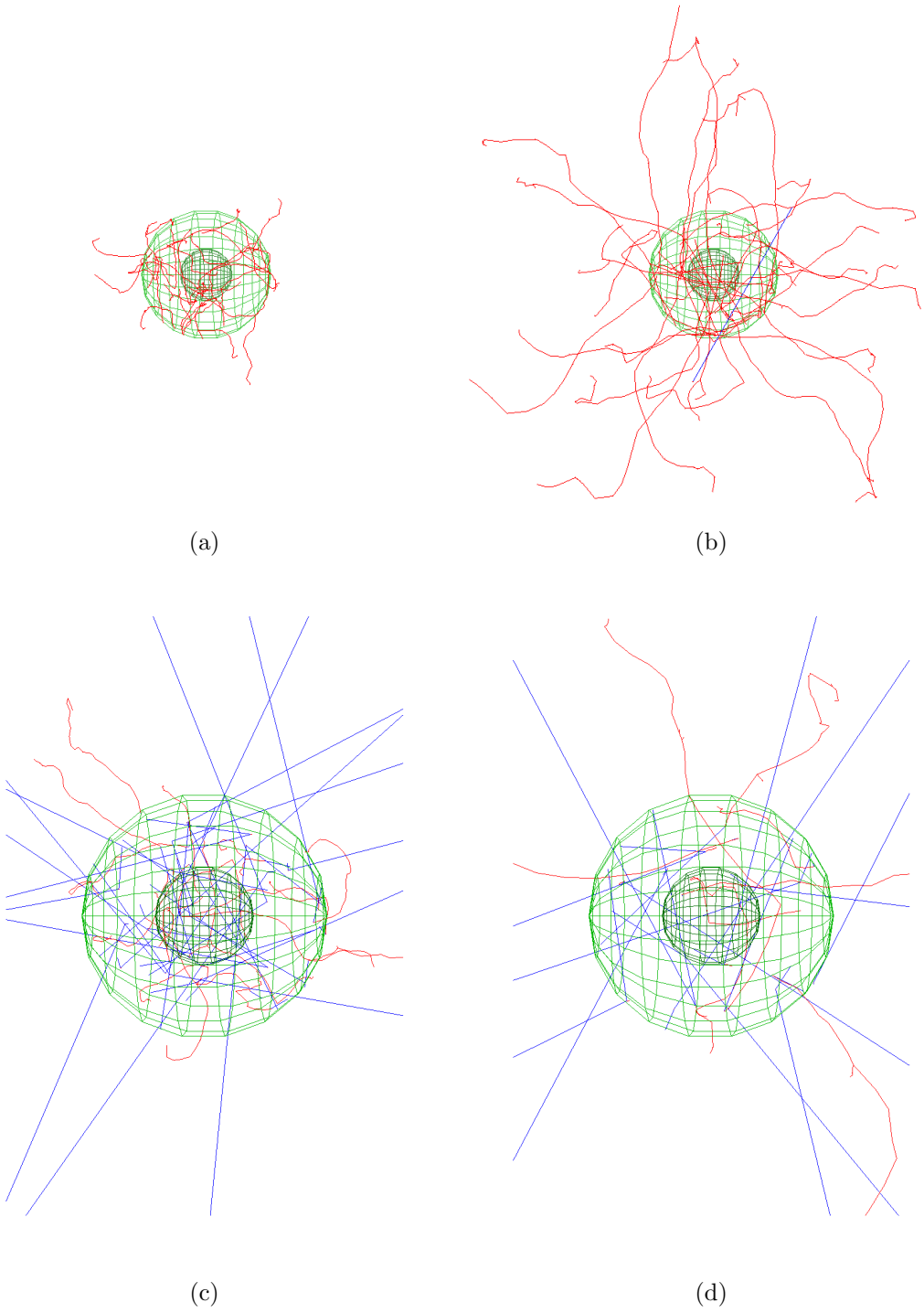

Figure 1. Electron and photon track structures in a homogeneous water cell showing the cell and surrounding water. The cytoplasm geometry is shown in light green, the nucleus geometry in dark green, electron tracks in red and photon tracks in blue. Particles are incident uniformly across the cell surface and in random directions. (a) 20 keV incident electrons, 30 particles; (b) 40 keV incident electrons, 30 particles; (c) 20 keV incident photons, 50 events; (d) 40 keV incident photons, 19 events. Only photon tracks which had an interaction within the cell are shown, from 150,000 primary particles.

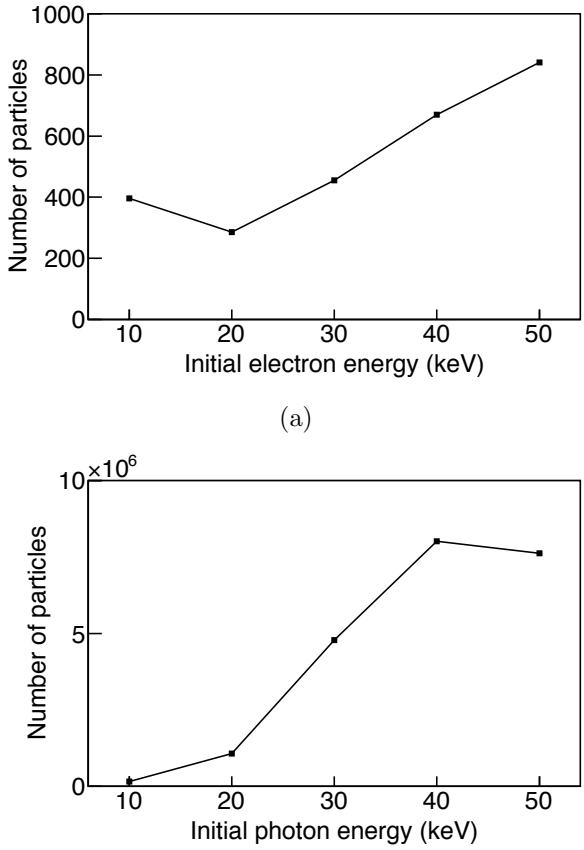

Figure 2. Number of incident particles needed to deposit 3 MeV in the reference cell as a function of initial particle energy for (a) electrons and (b) photons.

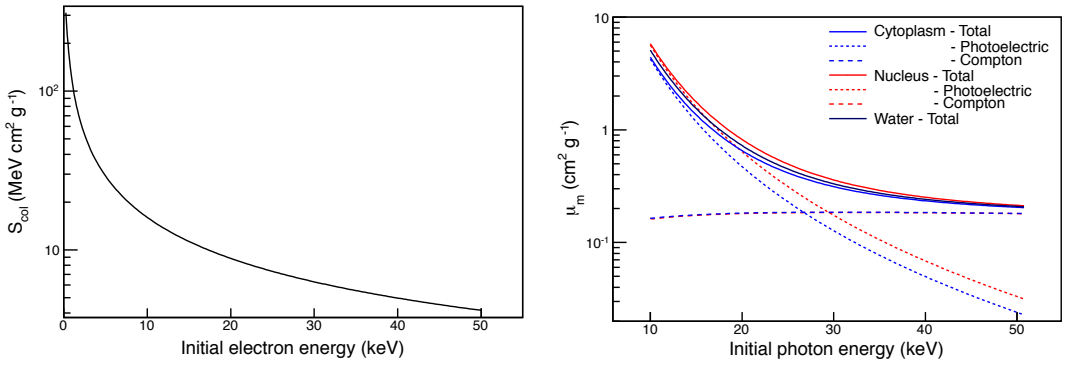

Figure 3. (a) Electron mass collision stopping power (S_{col}) in the cytoplasm used by the Penelope electromagnetic models in Geant4 (the stopping powers in nucleus material and liquid water are identical viewed on this scale). (b) Photon mass attenuation coefficient (μ_m) in the cytoplasm and nucleus materials and liquid water used by the Penelope electromagnetic models in Geant4.

3. Results

3.1. Ionisations

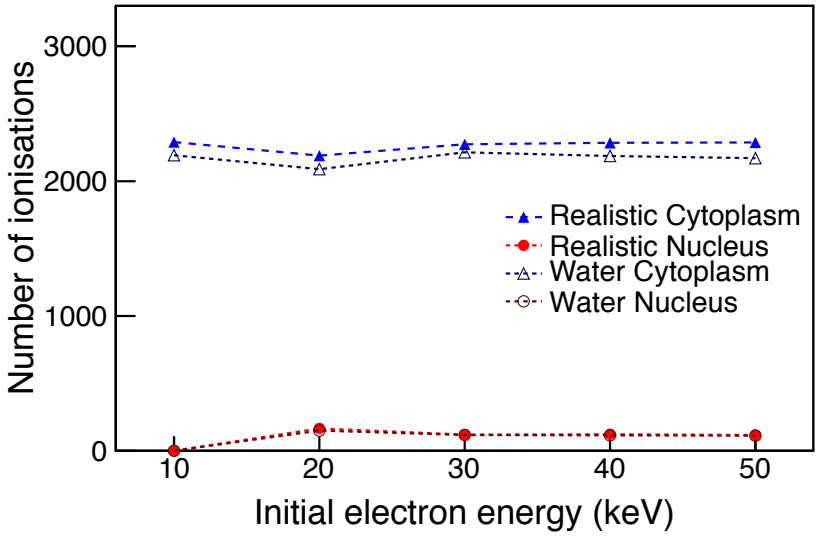

(a)

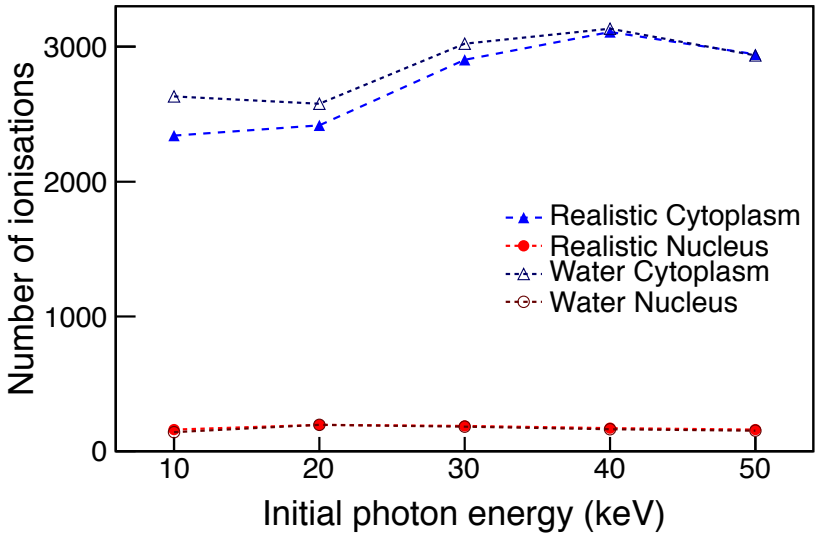

(b)

Figure 4. Number of ionisations in the reference cell filled with realistic materials or liquid water as a function of incident particle energy for (a) electrons; (b) photons.

Figure 4 shows the number of ionisations in the cytoplasm and nucleus in the reference cell (with density $1.0\,\mathrm{g\,cm^{-3}}$ and with nucleus radius $2\,\mu$m). Data is shown for the realistic cytoplasm and nucleus materials and for the case of the model cell filled entirely with liquid water. The vast majority of ionisations occur in the cytoplasm with $\lesssim 10\,\%$ occuring in the nucleus. This can be attributed to the small fractional volume

of the nucleus and the low dose of irradiation.

Figure 4(a) shows that for incident electrons there is very little change in ionisations produced when the realistic cytoplasm and nucleus compositions are replaced with liquid water, with differences typically $\lesssim 3\,\%$. This reflects the very similar stopping power for the materials. Figure 4(b) shows that for incident photons there is a progressively lower number of ionisations produced in the cytoplasm material compared to liquid water towards lower photon energies. This reflects the differences in the attenuation coefficients for these material compositions towards lower energies (c.f. figure 3(b)). The differences in number of ionisations in the nucleus region are not above statistical variation.

We note, however, that the 250 eV low energy limit of the Low Energy electromagnetic (Penelope) models means that secondary particles that would otherwise be produced below this threshold are not tracked, but recorded as a local energy deposit. Hence, the large number of ionisations that are produced by secondary electrons with energies below 250 eV are not explicitly recorded in the simulations. In the following, therefore, we show results for energy deposition rather than number of ionisations.

3.2. Density

Figure 5 shows energy deposited in the cell by incident electrons when the cytoplasm density increases from 0.5 to 2.0 $\mathrm{g\,cm^{-3}}$ normalised to the total energy deposit in the 1.0 $\mathrm{g\,cm^{-3}}$ case. Figure 6 shows corresponding electron tracks. Figures 7 and 8 show the corresponding results for photons. The total energy deposit SEM is less than 1 %; the error bars are too small to display on the plots.

The effect of changing the nucleus density was also investigated. However, because the nucleus occupies a small proportion of the total cell volume ($\lesssim 10\,\%$), the changes in energy deposit were found to be negligible and results are not shown here.

For 10 keV electrons, the energy deposit in the cell is not affected by changing cytoplasm density as nearly all electrons at this energy are stopped within the cell and deposit all their energy. At all other incident energies, the total deposited energy increases with density. Incident 20 keV electrons show a geometry dependent saturation effect — as the density increases all electrons are eventually stopped within the cell and no further increase in energy deposit occurs with increasing density. Thus, a higher density cytoplasm can slow down higher energy electrons in a similar manner to lower energy electrons in a less dense cell. This can also be seen by comparing the track structure for 50 keV electrons in 2.0 $\mathrm{g\,cm^{-3}}$ density cytoplasm with the tracks for 30 keV electrons in 0.5 $\mathrm{g\,cm^{-3}}$ density in figure 6(a) and (d). At incident electron energies $\gtrsim 30$ keV, the trend in energy deposition with density is approximately linear, reflecting the dependence on probability of interactions.

For photons, a similar trend is observed in energy deposition changes with cytoplasm density (figure 7), whereby an increased cytoplasm density leads to more primary interactions and more energy deposited by secondary electrons. Significant

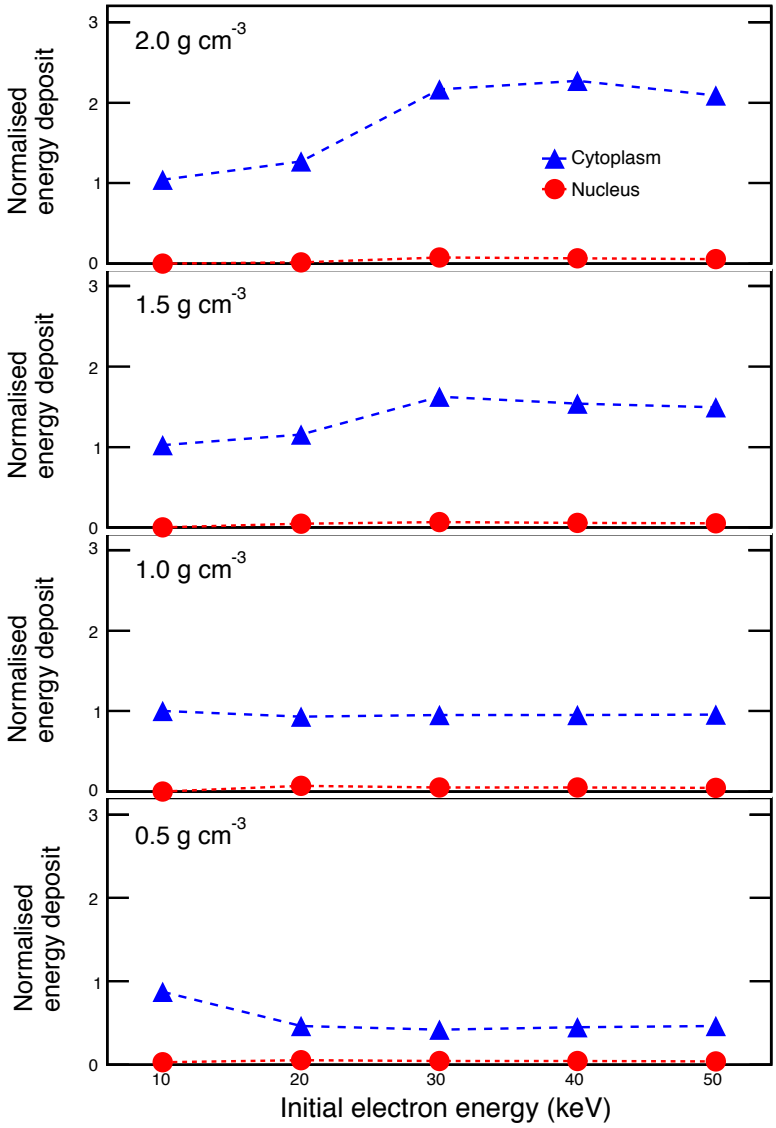

Figure 5. Energy deposited by electrons in the cytoplasm and nucleus when the cytoplasm density is varied over the range 0.5–2.0 g cm^{-3}. The energy deposit is normalised to the 1.0 g cm^{-3} case.

non-linearity is evident at 30 keV, which can be attributed to more secondary electrons stopping and depositing their energy within the denser cell rather than traversing and escaping the cell. This can be seen from figure 8, which shows tracks for 30 keV incident photons and secondary electrons for two different cytoplasm densities. The increase in the number of secondary electrons with cytoplasm density is clearly visible, as is the reduced secondary electron mean track lengths leading to more electrons stopping within the cell. At higher densities, we would anticipate a similar non-linear increase for 40 and 50 keV incident photons.

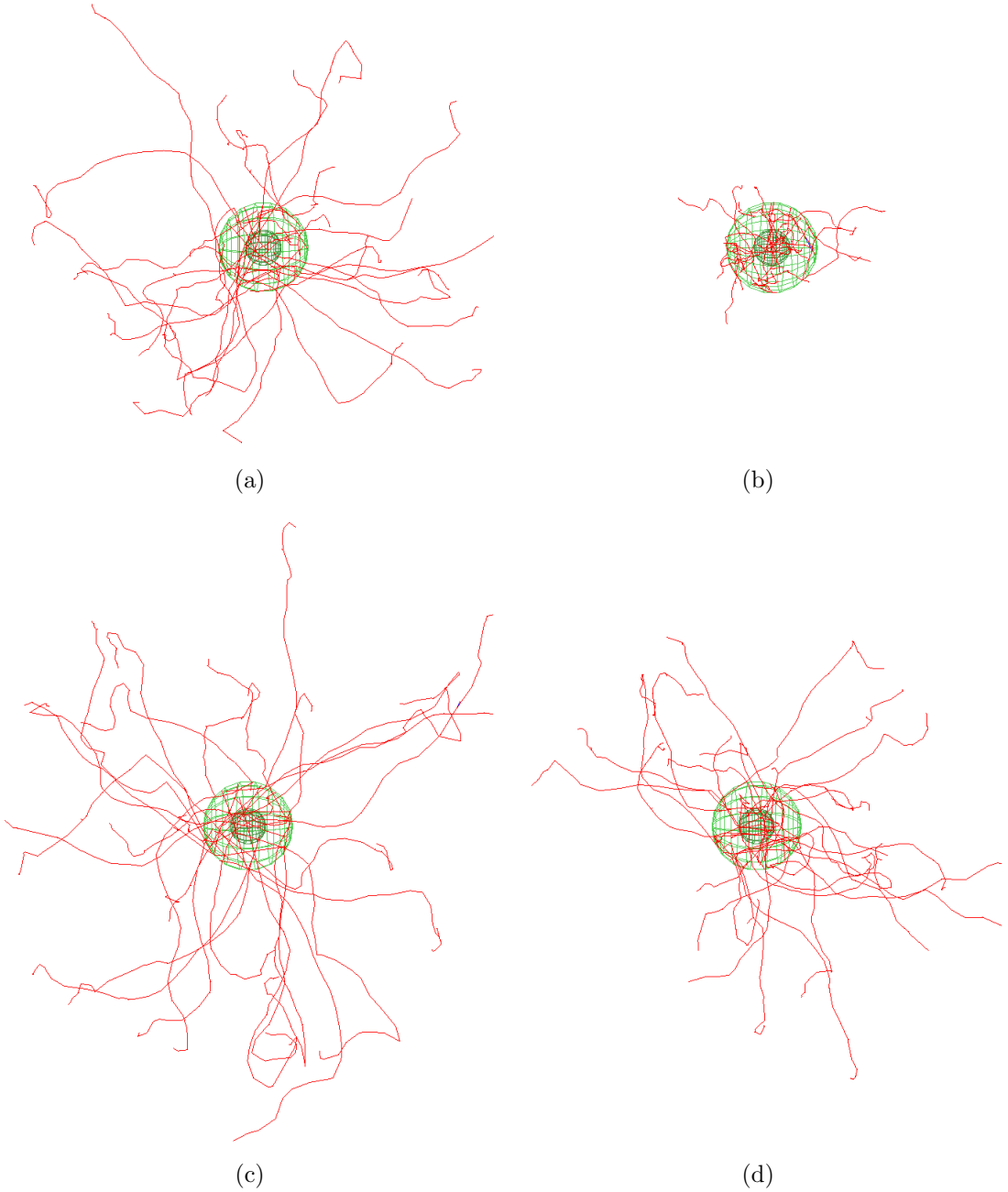

Figure 6. Electron tracks (red) in the cell model with increasing cytoplasm density, 30 particles: (a) 30 keV electrons in 0.5 g cm^{-3}; (b) 30 keV electrons in 2.0 g cm^{-3}; (c) 50 keV electrons in 0.5 g cm^{-3}; (d) 50 keV electrons in 2.0 g cm^{-3}.

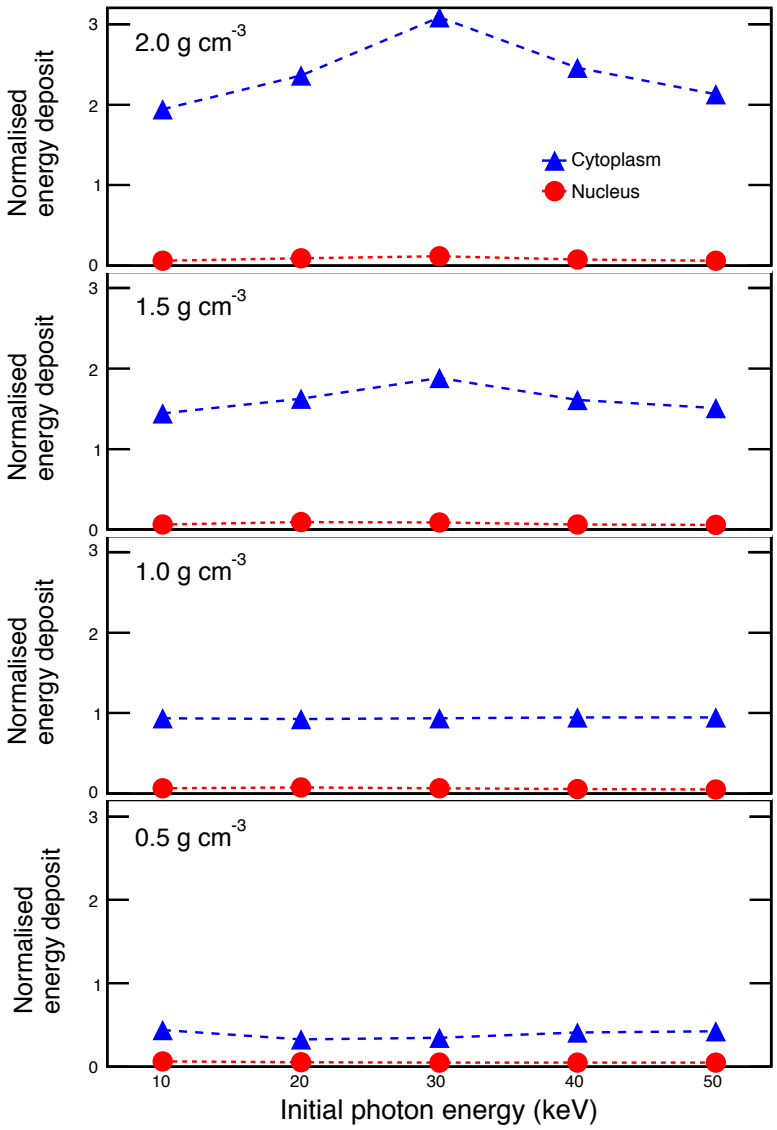

Figure 7. Energy deposited by photons in the cytoplasm and nucleus when the cytoplasm density is varied over the range 0.5–2.0 g cm^{-3}. The energy deposit is normalised to the 1.0 g cm^{-3} case.

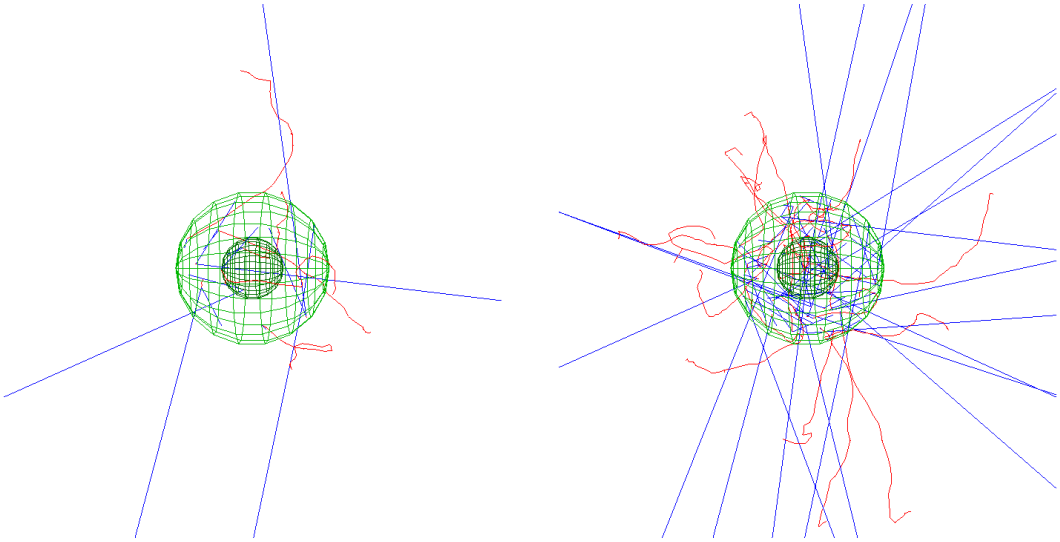

(a) (b)

Figure 8. 30 keV photon tracks (blue) and secondary electron tracks (red) in the cell model with increasing cytoplasm density. a) $0.5\,\mathrm{g\,cm^{-3}}$, 10 events; (b) $2.0\,\mathrm{g\,cm^{-3}}$, 44 events. Only photon tracks which had an interaction within the cell are shown, from 150,000 primary particles.

3.3. Nucleus Volume

Figures 9 and 11 show energy deposited in the cell model by incident electrons and photons, respectively, as the size of the nucleus was successively doubled until it was 8 times its original volume and accounted for over half the total volume of the cell. The total energy deposit SEM is less than 1 % and the error bars are too small to display on the plots. Figure 10 shows a corresponding visualisation of electron tracks.

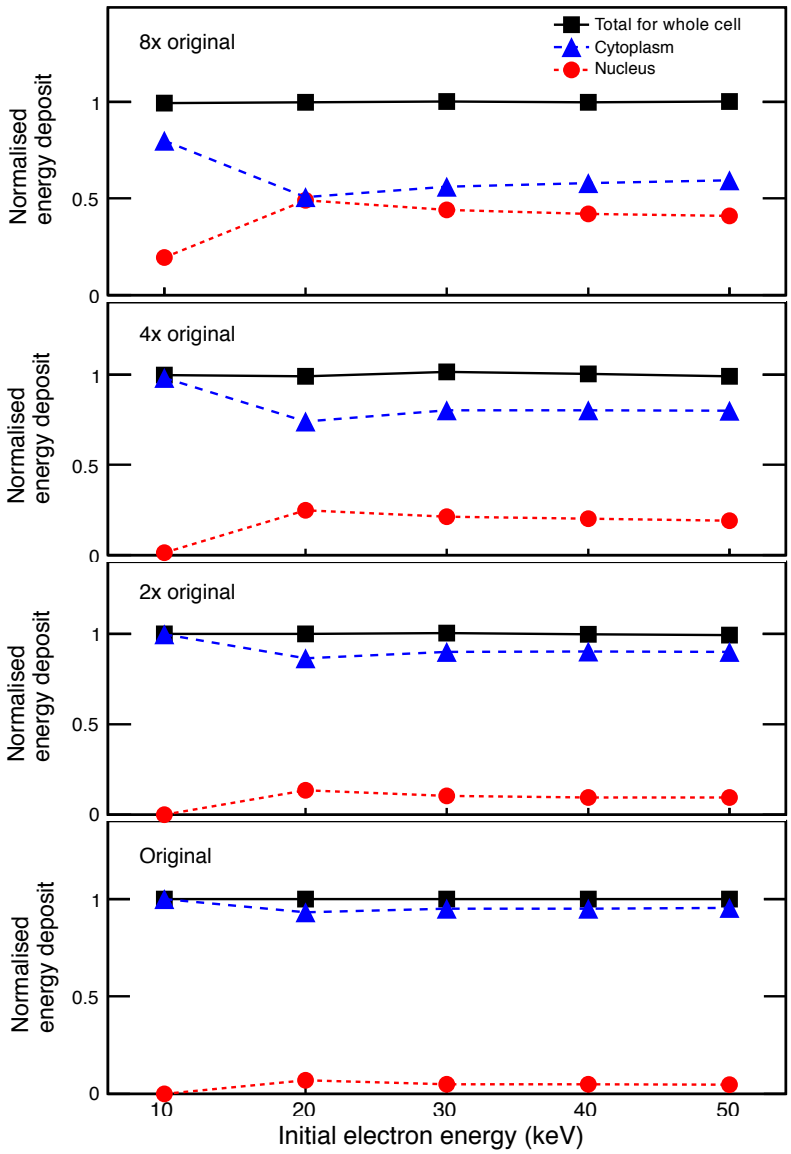

Figure 9. Energy deposited by electrons in the whole cell, cytoplasm only or nucleus only when the volume of nucleus is increased up to 8 × its original volume

For electrons, as the nucleus volume increases the proportion of energy deposited in the nucleus increases, with a corresponding decrease in that deposited in the cytoplasm. When the nucleus is 8 times its original volume and occupies $\simeq$ 50 % of the total cell

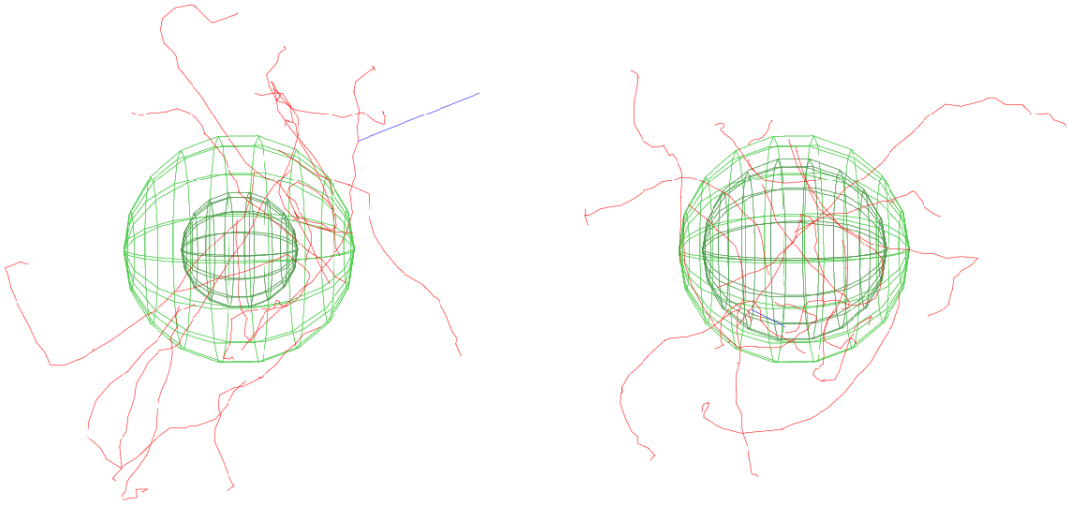

(a) (b)

Figure 10. 30 keV electron tracks (red) in the cell model with increasing nucleus volume: (a) cell with 2 × original nucleus volume; (b) cell with 8 × original nucleus volume.

volume, the energy deposited in the nucleus by 10 keV electrons still remains less than that deposited in the cytoplasm as the electrons do not all penetrate far enough into the cell to reach the nucleus. Similarly at higher electron energies, the energy deposit in the nucleus is still less than that in the cytoplasm. Particles which traverse the whole cell, including the nucleus, still have a significant portion of their path length in the cytoplasm. In addition, some particles are injected at a very shallow angle relative to the cell surface, only traversing the cytoplasm before leaving the cell. These geometric effects are moderated for 20 keV electrons which are likely to be stopped within the nucleus before reaching cytoplasm on the opposite side of the cell to where they entered, and which are more likely than higher energy electrons to scatter into the nucleus if injected at a shallow angle.

Similarly to electrons, increasing the nuclear volume leads to greater energy deposit by photons in the nucleus. For photons, when the nucleus is 8 times its original volume, the energy deposit in the nucleus nearly matches that in the cytoplasm at the higher energies investigated (40, 50 keV) and at the lower energies (10, 20, 30 keV) exceeds that of cytoplasm due to the higher μ_m in nucleus material at lower energies (c.f. figure 3(b)). A similar trend is also seen in the total energy deposit by photons, due to the difference in μ_m for nucleus and cytoplasm materials.

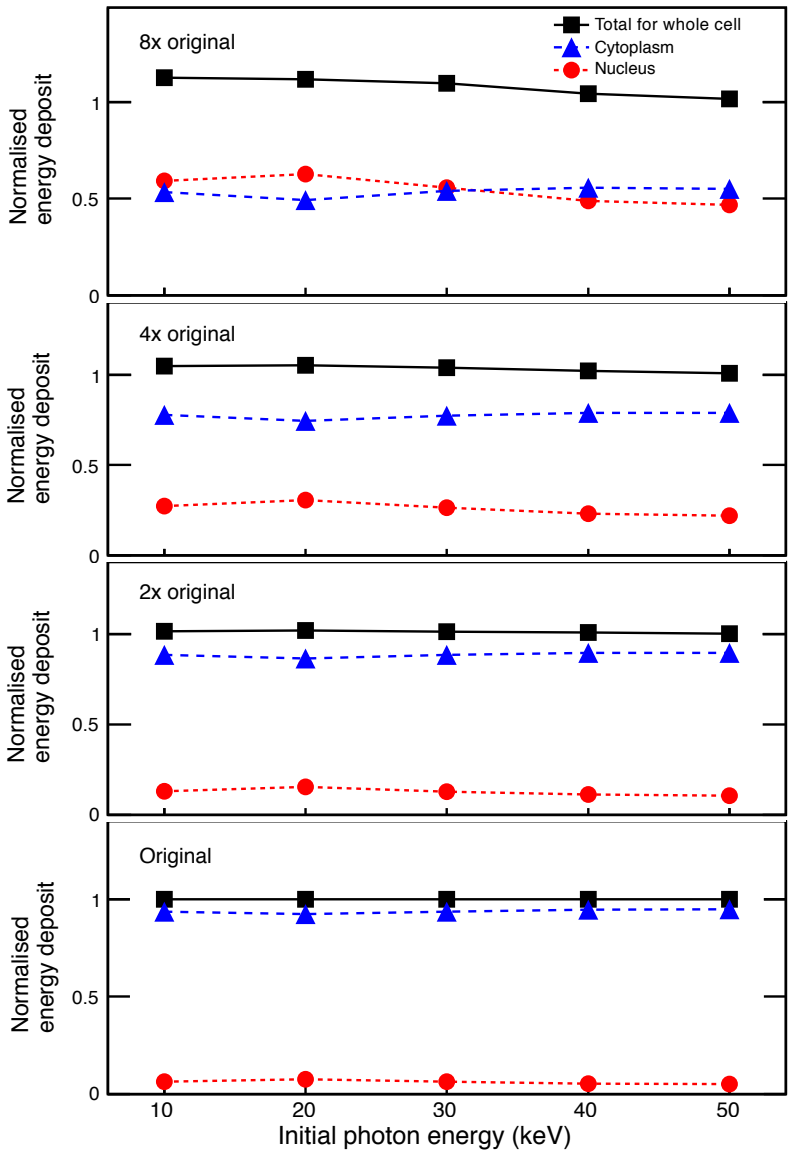

Figure 11. Energy deposited by photons in the whole cell, cytoplasm only or nucleus only when the volume of nucleus is increased up to 8 × its original volume.

4. Discussion

Our results demonstrate that cells immersed in a low-dose radiation bath, such as healthy cells in an out-of-field radiotherapy scenario, experience only a relatively small proportion of ionisations in their nucleus, with the number of ionisations in the cytoplasm typically at least an order of magnitude larger. Since every ionisation can produce a potentially harmful free radical that can contribute to triggering damage response signalling pathways via organelles in the cytoplasm, this suggests that the cytoplasm is a more relevant target than nuclear DNA when considering radiation damage to normal tissue. Damage response signalling pathways initiated outside the nucleus can lead to nuclear DNA damage by signalling across the nuclear membrane (Rodemann and Blaese, 2007). Oxidative damage to extra-nuclear (mitochondrial) DNA and RNA can disrupt mitochondrial function which may result in genomic instability or complex diseases such as heart disease (Rosenberg, 2004; Dayal et al., 2009) and intracellular oxidative stress is thought to be sufficient to cause cell death for example through liberation of Ca^{2+} ions (Usami et al., 2008). Furthermore, mitochondrial apoptosis is a receptor-mediated pathway triggered primarily by intracellular stresses (Kim et al., 2005) and so is a viable candidate for explaining the bystander effect, where cells not directly exposed to irradiation exhibit truncated survival when in close proximity to cells exposed to radiation (Prise et al., 2005; Zhou et al., 2008; Prise and O'Sullivan, 2009).

In this study, we found that subcellular heterogeneity in chemical composition can affect the number of ionisations produced by incident photons due to non-negligible differences in μ_m at low photon energies ($\leq$ 30 keV). For incident electrons on the other hand, the negligible differences in S_{col} for the different materials (cytoplasm, nucleus, water) produced correspondingly negligible differences in number of ionisations produced. However, the effect of sub-micron scale chemical heterogeneities cannot be ruled out as a significant factor in Monte Carlo radiation damage simulations until more information is available, including better specification of the chemical composition of sub-cellular components and the cytosol. As noted previously, the Low Energy Physics models used in these simulations employ a condensed history approach with the cut-off for production of secondaries set to 250 eV, so the ionisations produced by very low energy electrons cannot be explicitly simulated. The very low energy models in Geant4-DNA (Chauvie et al., 2006, 2007; Incerti et al., 2010) track every interaction discretely. However, Geant4-DNA is currently only available for liquid water and so cannot be used to investigate the effect of chemical composition. Nevertheless, a test simulation of our homogeneous water cell model with Geant4-DNA revealed that the number of ionisations produced was 3 orders of magnitude higher than that calculated by the Low Energy models with a 250 eV production cutoff. This indicates that for a 1 Gy dose, approximately 250,000 ionisations may occur in the nucleus, which is comparable to estimates reported in previous studies (e.g. Goodhead (1994)). The number of ionizations in the cytoplasm, on the other hand is an order of magnitude

higher and thus, there can be a dominant contribution from intra-cellular signaling to the overall probability of DNA and other biochemical damage. We posit that the rapid increase in number of ionisations produced below 250 eV should follow a non-linear trend with chemical composition and the number of valence shell electrons. Hence chemical composition could have a more significant effect on the number of ionisations than can currently be simulated. The number of ionisations itself is not sufficient to draw firm conclusions on biological outcomes. The spatial clustering of ionisations determines the likelihood of directly damaging DNA and provides the link between simulation results and experimental evidence, although significant challenges remain (Nikjoo et al., 1999; Prise et al., 2001; Hada and Georgakilas, 2008). While studies to date have focused exclusively on cluster damage to DNA in the nucleus, ionisation clustering outside the nucleus can be an important indicator for mitochondrial DNA and RNA damage also. It is becoming apparent that low LET radiation such as that used in this study can produce ionisation clusters capable of causing simple and complex DNA damage, in a similar fashion to high LET radiation (Nikjoo and Lindborg, 2010; McNamara et al., 2012). A major limitation of cluster studies at low doses, however, is that the number of energy deposition events that occur in nanometric volumes is insufficient to quantitatively evaluate DNA damage and repair mechanisms.

Another limitation of current Monte Carlo simulations of very low energy electrons is that the interactions are modelled using atomic cross-sections which do not properly take into account the soft condensed (liquid) phase of the biological target. An improved treatment of low-energy electromagnetic interactions in biological molecules (including water) will likely require a hybrid Monte Carlo – molecular dynamics approach, including collective effects, inter- and intra-molecular forces at very low energies (Heller et al., 1974; Fano, 1992).

This study has revealed the important and interrelated effects that cell geometry and microstructure have on radiation damage. We found nonlinear trends in energy deposition with variations in cytoplasm density due to cell geometry. Our simulations also showed significant dependence of energy deposition on geometry when the mean path length of primary and secondary electrons is comparable to cell size. In particular, the nucleus size was shown to govern energy deposition in the nucleus, and so potentially able to cause DNA damage, as distinct from ionisations in the cytoplasm which could potentially trigger other damage responses via cell signalling. These results could have important implications for radiosensitivity dependence on cell cycle and cell type, which are not normally considered in radiobiological models for cell kill or normal tissue complications (Zaider and Wuu, 1995; Marples et al., 2004).

This study has focused on ionisations and energy deposition in a single cell with minimal substructure; future work will include incorporating additional cellular substructure, such as organelles and membranes. An important extension of this model is to simulate cell populations, to mimic a tissue-scale environment. Of particular interest is to compare the effects caused by low-LET and high-LET radiation at low-doses, since in the high-LET case, radiation might not reach every cell. This will enable

us to study bystander effects as well as ionization clustering. (Although we note that very low energy electrons can mimic the ionisation clustering behaviour characteristic of high-LET radiation.) Additional work is also needed to link the ionisation distribution to biological outcome. This will require modelling the chemical evolution of initial free radical products and the diffusion of chemical species. Along with a consideration of cellular repair mechanisms, this would give much needed insight into the wide range of responses seen post-irradiation. Current developments are underway in Geant4-DNA to model water radiolysis and the post-irradiation chemical phase (Karamitros et al., 2011).

5. Conclusions

In a low-dose radiation bath, the cytoplasm in a typical cell attracts a disproportionate number of ionisations and amount of energy deposition, relative to the nucleus. This signifies that the cytoplasm and organelles therein may be important targets for radiation damage, implying consequences for healthy cells exposed to out-of-field regions in external beam radiotherapy treatments. This warrants investigation as much as the conventional focus of nuclear DNA damage to unhealthy (tumour) cells targeted by high-dose radiation.

Our results demonstrate the importance of accurate specification of cell type and subcellular components in microdosimetry simulations. We have shown that bulk density has a significant effect on energy deposition, but this is also influenced by cell geometry, particularly when the particle energies considered correspond to electron path lengths of the order of the cellular size. Cellular heterogeneity should also be considered as denser subregions in a cell can slow down higher energy electrons in a similar manner to lower energy electrons in less dense subregions.

The region in which ionisations occur within a cell is influenced by the volume of nucleus relative to that of cytoplasm, and so this could be a distinguishing factor in identifying different cellular responses triggered from distinct subregions of a cell.

Acknowledgments

HL Byrne acknowledges funding from an Australian Postgraduate Award. The authors acknowledge the Cancer Institute of NSW for funding the Advanced Computing Facility for Cancer Research, which was used for these simulations. Sebastien Incerti and Vladimir Ivanchenko of the Geant4 consortium are also greatly acknowledged for their technical expertise.

References

Agostinelli S et al. 2003 GEANT4-a simulation toolkit *Nucl. Instrum. Meth. A* **506**(3), 250–303.

Ahmed K M, Fan M, Nantajit D, Cao N and Li J J 2008 Cyclin D1 in low-dose radiation-induced adaptive resistance *Oncogene* **27**(53), 6738–48.

Allison J et al. 2006 Geant4 developments and applications *IEEE Trans. Nuc. Sci.* **53**(1), 270–78.

Averbeck D 2010 Non-targeted effects as a paradigm breaking evidence *Mut. Res.* **687**(1-2), 7–12.

Baró J, Sempau J, Fernàndez-Varea J and Salvat F 1995 PENELOPE: an algorithm for monte carlo simulation of the penetration and energy loss of electrons and positrons in matter *Nucl. Instrum. Meth. B* **100**(1), 31–46.

Bassing C H and Alt F W 2004 The cellular response to general and programmed DNA double strand breaks *DNA Repair* **3**(89), 781–96.

Battlehner C, Saldiva P, Carvalho C, Takagaki T, Montes G, Younes R and Capelozzi V 1993 Nuclear cytoplasmic ratio correlates strongly with survival in non-disseminated neuroendocrine carcinoma of the lung *Histopathology* **22**(1), 31–34.

Chauvie S, Francis Z, Guatelli S, Incerti S, Mascialino B, Montarou G, Moretto P, Nieminen P and Pia M G 2006 Monte Carlo simulation of interactions of radiation with biological systems at the cellular and DNA levels: The Geant4-DNA project *Radiat. Res.* **166**(4), 676–77.

Chauvie S, Francis Z, Guatelli S, Incerti S, Mascialino B, Moretto P, Nieminen P and Pia M 2007 Geant4 physics processes for microdosimetry simulation: Design foundation and implementation of the first set of models *IEEE T. Nucl. Sci.* **54**(6), 2619–28.

Chauvie S et al. 2004 *in* J. A Seibert, ed., '2004 IEEE Nuclear Science Symposium Conference Record, Vols 1-7' IEEE New York pp. 1881–85.

Chofor N, Harder D, Rhmann A, Willborn K C, Wiezorek T and Poppe B 2010 Experimental study on photon-beam peripheral doses, their components and some possibilities for their reduction *Phys. Med. Biol.* **55**(14), 4011–27.

Chouin N, Bernardeau K, Bardies M, Faivre-Chauvet A, Bourgeois M, Apostolidis C, Morgenstern A, Lisbona A, Cherel M and Davodeau E 2009 Evidence of extranuclear cell sensitivity to alpha-particle radiation using a microdosimetric model. II. Application of the microdosimetric model to experimental results *Radiat. Res.* **171**(6), 664–73.

Dayal D et al. 2009 Mitochondrial complex II dysfunction can contribute significantly to genomic instability after exposure to ionizing radiation *Radiat. Res.* **172**(6), 737–45.

Elkind M M 1985 DNA damage and cell killing cause and effect? *Cancer* **56**(10), 2351–63.

Fano U 1992 A common mechanism of collective phenomena *Rev. Mod. Phys.* **64**(1), 313–19.

Francis Z, Incerti S, Karamitros M, Tran H N and Villagrasa C 2011a Stopping power and ranges of electrons, protons and alpha particles in liquid water using the geant4-DNA package *Nucl. Instrum. Meth. B* **269**(20), 2307–11.

Francis Z, Villagrasa C and Clairand I 2011b Simulation of DNA damage clustering after proton irradiation using an adapted DBSCAN algorithm *Comput. Meth. Prog. Bio.* **101**(3), 265–70.

Friedland W, Jacob P, Bernhardt P, Paretzke H G and Dingfelder M 2003 Simulation of DNA damage after proton irradiation *Radiat. Res.* **159**(3), 401–10.

Garty G, Schulte R, Shchemelinin S, Leloup C, Assaf G, Breskin A, Chechik R, Bashkirov V, Milligan J and Grosswendt B 2010 A nanodosimetric model of radiation-induced clustered DNA damage yields *Phys. Med. Biol.* **55**(3), 761–81.

Goodhead D T 1994 Initial events in the cellular effects of ionizing radiations: Clustered damage in DNA *Int. J. Radiat. Biol.* **65**(1), 7–17.

Hada M and Georgakilas A G 2008 Formation of clustered DNA damage after high-LET irradiation: A review *J. Radiat. Res.* **49**(3), 203–10.

Hall E J 2006 Intensity-modulated radiation therapy, protons, and the risk of second cancers *Int. J. Radiat. Oncol.* **65**(1), 1–7.

Hall E J and Wuu C S 2003 Radiation-induced second cancers: The impact of 3D-CRT and IMRT *Int. J. Radiat. Oncol.* **56**(1), 83–88.

Hamada N, Matsumoto H, Hara T and Kobayashi Y 2007 Intercellular and intracellular signaling pathways mediating ionizing radiation-induced bystander effects *J. Radiat. Res.* **48**(2), 87–95.

Hei T K, Ballas L K, Brenner D J and Geard C R 2009 Advances in radiobiological studies using a microbeam *J. Radiat. Res.* **50**(Suppl.A), A7–A12.

Heller J M, Hamm R N, Birkhoff R D and Painter L R 1974 Collective oscillation in liquid water *J. Chem. Phys.* **60**(9), 3483–86.

Hsiao Y and Stewart R D 2008 Monte carlo simulation of DNA damage induction by x-rays and selected radioisotopes *Phys. Med. Biol.* **53**(1), 233–44.

Incerti S et al. 2010 Comparison of GEANT4 very low energy cross section models with experimental data in water *Med. Phys.* **37**(9), 4692–708.

International Commission on Radiation Units and Measurements (ICRU) 1989 *Tissue Substitutes in Radiation Dosimetry and Measurement* ICRU Report 44: ICRU Publications Bethesda, Maryland.

Karamitros M et al. 2011 Modeling radiation chemistry in the Geant4 toolkit *Prog. Nucl. Sci. Tec.* **2**, 503–08.

Kim R, Emi M and Tanabe K 2005 Role of mitochondria as the gardens of cell death *Cancer Chemoth. Pharm.* **57**(5), 545–53.

Kuncic Z, Byrne H L, McNamara A L, Guatelli S, Domanova W and Incerti S 2012 In silico nanodosimetry: New insights into nontargeted biological responses to radiation *Comput. Math. Method M.* **2012**, 1–9.

Marples B, Wouters B G, Collis S J, Chalmers A J and Joiner M C 2004 Low-dose hyper-radiosensitivity: A consequence of ineffective cell cycle arrest of radiation-damaged G2-phase cells *Radiat. Res.* **161**(3), 247–55.

McNamara A L, Guatelli S, Prokopovich D A, Reinhard M I and Rosenfeld A B 2012 A comparison of x-ray and proton beam low energy secondary electron track structures using the low energy models of Geant4 *Int. J. Radiat. Biol.* **88**(1-2), 164–70.

Nikjoo H, Emfietzoglou D, Watanabe R and Uehara S 2008 Can Monte Carlo track structure codes reveal reaction mechanism in DNA damage and improve radiation therapy? *Radiat. Phys. and Chem.* **77**(1012), 1270–79.

Nikjoo H and Lindborg L 2010 RBE of low energy electrons and photons *Phys. Med. Biol.* **55**(10), R65–R109.

Nikjoo H, O'Neill P, Terrissol M and Goodhead D T 1999 Quantitative modelling of DNA damage using monte carlo track structure method *Radiat. Environ. Biophys.* **38**(1), 31–38.

Prise K M and O'Sullivan J M 2009 Radiation-induced bystander signalling in cancer therapy *Nat. Rev. Cancer* **9**(5), 351–60.

Prise K M, Pinto M, Newman H C and Michael B D 2001 A review of studies of ionizing radiation-induced double-strand break clustering *Radiat. Res.* **156**(5), 572–76.

Prise K M, Schettino G, Folkard M and Held K D 2005 New insights on cell death from radiation exposure *Lancet Oncol.* **6**(7), 520–28.

Rodemann H P and Blaese M A 2007 Responses of normal cells to ionizing radiation *Semin. Radiat. Oncol.* **17**(2), 81–88.

Rosenberg P 2004 Mitochondrial dysfunction and heart disease *Mitochondrion* **4**(56), 621–28.

Salvat F, Fernàndez-Varea J M and Sempau J 2009 PENELOPE-2008: a code system for monte carlo simulation of electron and photon transport *Issy-les-Moulineaux, France: OECD Nuclear Energy Agency* .
URL: *http://www.nea.fr*

Schettino G, Al Rashid S and Prise K 2010 Radiation microbeams as spatial and temporal probes of subcellular and tissue response *Mutat. Res.-Rev. Mutat.* **704**(1-3), 68–77.

Shao C 2004 Targeted cytoplasmic irradiation induces bystander responses *P. Natl. Acad. Sci. USA* **101**(37), 13495–500.

Syme A, Kirkby C, Mirzayans R, MacKenzie M, Field C and Fallone B G 2009 Relative biological damage and electron fluence in and out of a 6 MV photon field *Phys. Med. Biol.* **54**(21), 6623–33.

Usami N, Furusawa Y, Kobayashi K, Lacombe S, Reynaud-Angelin A, Sage E, Wu T, Croisy A, Guerquin-Kern J L and Le Sech C 2008 Mammalian cells loaded with platinum-containing molecules are sensitized to fast atomic ions *Int. J. Radiat. Biol.* **84**(7), 603–611.

Watanabe S, Okita K, Harada T, Kodama T, Numa Y, Takemoto T and Takahashi T 1983 Morphologic studies of the liver-cell dysplasia *Cancer* **51**(12), 2197–205.

White D, Woodard H and Hammond S 1987 Average soft-tissue and bone models for use in radiation-dosimetry *Brit. J. Radiol.* **60**(717), 907–13.

Wright E G 2010 Manifestations and mechanisms of non-targeted effects of ionizing radiation *Mutat. Res.-Fund. Mol. M.* **687**(1-2), 28–33.

Zaider M and Wuu C S 1995 The effects of sublethal damage recovery and cell cycle progression on the survival probability of cells exposed to radioactive sources *Brit. J. Radiol.* **68**(805), 58–63.

Zhou H, Ivanov V N, Lien Y C, Davidson M and Hei T K 2008 Mitochondrial function and nuclear factor-kB-mediated signaling in radiation-induced bystander effects *Cancer Res.* **68**(7), 2233–40.